

Dynamic Sparse Training with Structured Sparsity

Mike Lasby¹ Anna Golubeva^{2,3} Utku Evci⁴ Mihai Nica^{5,6} Yani Ioannou¹

Abstract

Dynamic Sparse Training (DST) methods achieve state-of-the-art results in sparse neural network training, matching the generalization of dense models while enabling sparse training and inference. Although the resulting models are highly sparse and theoretically cheaper to train, achieving speedups with unstructured sparsity on real-world hardware is challenging. In this work we propose a DST method to learn a variant of *structured* N:M sparsity, the acceleration of which in general is commonly supported in commodity hardware. Furthermore, we motivate with both a theoretical analysis and empirical results, the generalization performance of our specific N:M sparsity (constant fan-in), present a condensed representation with a reduced parameter and memory footprint, and demonstrate reduced inference time compared to dense models with a naive PyTorch CPU implementation of the condensed representation. Our source code is available at github.com/calgaryml/condensed-sparsity.

1. Introduction

Dynamic Sparse Training (DST) methods such as RigL (Evci et al., 2021) are the state-of-the-art in sparse training methods, learning *unstructured* Sparse Neural Networks (SNNs) with 85–95% fewer weights than dense models, while maintaining similar generalization. Furthermore, sparse training methods employ sparsity *both during training and inference*, unlike pruning and other methods (Zhou et al., 2021) that only exploit sparsity at inference time.

While models trained with DST methods are highly sparse and enable a large reduction in theoretically computed Floating Point Operations (FLOPs), realizing similar speedups on hardware is challenging with unstructured

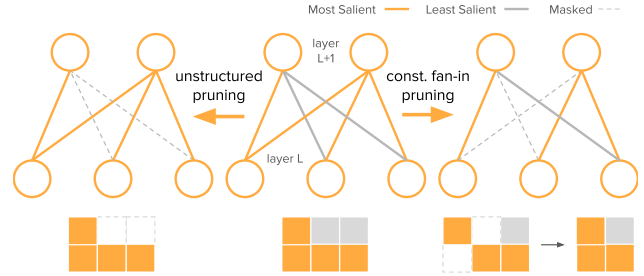


Figure 1: Constant fan-in pruning keeps the most salient weights *per neuron*, while unstructured pruning keeps the most salient weights *per layer*. A constant fan-in weight matrix has the same number of non-zero elements (here 2) per column allowing condensed representation. While pruning may remove salient weights affecting generalization, with SRigL structure and weights are learned concurrently.

sparsity. Structured sparsity realizes much higher gains in acceleration on real-world hardware for a given sparsity than unstructured sparsity in practice, even considering recent advances in accelerating unstructured SNNs (Gale et al., 2020; Elsen et al., 2020). On the other hand, structured sparse pruning can remove salient weights, typically resulting in worse generalization than comparable unstructured SNNs for the same sparsity level (Fig. 1).

Our work presents a best-of-both-worlds approach, by exploiting the DST framework to learn *both* a highly-sparse *and* structured representation, while maintaining the generalization performance of DST and dense baselines. In summary our work presents the following novel contributions:

1. We propose a novel DST method, Structured RigL (SRigL), based on RigL (Evci et al., 2021). SRigL learns a SNN with constant fan-in structured sparsity (Fig. 1) while maintaining generalization comparable with RigL up to a high sparsity level (90%). This structure is a particular case of “N:M sparsity” which requires N out of M consecutive weights to be non-zero (Nvidia, 2020).
2. Our empirical analysis shows that at sparsity levels >90% RigL ablates whole neurons. By allowing ablation in SRigL, we can match the generalization performance of RigL even in this high-sparsity regime.
3. We motivate our choice of structure with a theoretical analysis of SNN output norm variance—a property related to training stability—and find that the constant fan-in constraint does not have a negative effect.

¹University of Calgary ²Massachusetts Institute of Technology

³The NSF AI Institute for Artificial Intelligence and Fundamental Interactions ⁴Google Brain ⁵University of Guelph ⁶Vector Institute.
@text Correspondence to: Mike Lasby <mklasby@ucalgary.ca>, Yani Ioannou <yani.ioannou@ucalgary.ca>.

4. We demonstrate that, similar to other N:M sparsity variants (Nvidia, 2020), our constant fan-in sparsity enables a compact representation that is not only parameter- and memory-efficient, but also amenable to real-world acceleration. While hardware support for our specific form of N:M sparsity is not yet available, we observe increased performance with highly sparse networks over dense baseline at inference time even with only a naive PyTorch CPU implementation.

2. Related Work

Dynamic Sparse Training Unlike with pruning, where weights are typically pruned after the dense network was trained (Han et al., 2015; 2016), or at initialization (Wang et al., 2020), DST methods learn the sparse connectivity among the neurons during training by periodically adding and removing weights based on various saliency criteria. For instance, Sparse Evolutionary Training (SET) (Mocanu et al., 2018) removes weights with the smallest magnitude and adds weights randomly; similarly, RigL (Evci et al., 2021) prunes weights with the smallest magnitude and regrows weights that have large-magnitude gradients. RigL has been shown to learn models with 95% fewer parameters than dense baselines, while maintaining the same generalization performance. Liu et al. (2021b) further improved the original RigL results by increasing the extent of the parameter space explored by modifying the sparse connectivity update schedule and drop rate.

While DST methods are highly effective at finding SNNs which reduce theoretical inference cost, they result in unstructured SNNs which are difficult to accelerate in practice due to various restrictions of common hardware architectures.

Accelerating Unstructured Sparse Neural Networks

Elsen et al. (2020) proposed a method for accelerating unstructured SNNs based on one-dimensional tiling of non-zero elements, which demonstrated significant speedups on both CPU (Elsen et al., 2020) and Graphics Processing Unit (GPU) (Gale et al., 2020). However, like most approaches to accelerating unstructured SNNs, this method relies on imposing structure on an existing sparse weight matrix *after training*. Our method can be considered a way of adding structure to SNNs *during training*, allowing the model to maximally utilize non-zero weights since structure and weights are learned concurrently.

Learning Block Structured Sparsity From Scratch

Spurred by the successes of DST in learning unstructured sparse models, recent works have attempted to apply DST principles to learn block-structured sparsity (Jiang et al., 2022; Dietrich et al., 2022). Block sparsity is a particular type of structured sparsity in which blocks of non-zero weights

are grouped together in arrangements that reduce the memory overhead required to store the indices of the non-zero weights. As the block size increases, better compression is achieved, but generalization performance decreases (Jiang et al., 2022; Zhou et al., 2021). Blocks can be generated out of contiguous weights in 1D or 2D or by utilizing a fixed number of non-zero weights per row or column group in the case of block-balanced sparsity (Hoefler et al., 2021). Dietrich et al. (2022) applied a modified variant of RigL to BERT models (Devlin et al., 2019). The resulting method is capable of learning models with block-structured sparsity. The authors demonstrated improvements in generalization performance at reduced FLOPs compared to a dense network baseline. Jiang et al. (2022) introduced a DST algorithm to reshuffle weights into a block sparsity pattern after sparse connectivity updates. Wall-clock speed-ups of up to four-times were reported with this method; however, generalization performance was reduced compared to RigL at comparable sparsities.

Learning N:M Structured Sparsity from Scratch

N:M sparsity is a specific form of block-balanced sparsity in which 1D blocks with M contiguous elements contain exactly N non-zero elements. N:M sparsity is particularly amenable to acceleration and several attempts have been made to train models with N:M fine-grained structure using DST methods. Yang et al. (2022) extended the DST method proposed by Liu et al. (2021a) to train multiple sparse sub-networks sampled from a single dense super-network. Their proposed method, Alternating Sparse Training (AST), switches the network topology between sparse sub-networks after each mini-batch during training. Yang et al. (2022) demonstrated state-of-the-art performance on several typical sparse training benchmarks. However, the DST methodology used in (Liu et al., 2021a) gradually increases sparsity during training to yield the desired sparsity at the end of training. Therefore, the dense model weights and gradients are required throughout the majority of training, greatly increasing the overall compute and storage requirements. While AST demonstrated a tantalizing possibility of training multiple sparse sub-networks within a single training loop, the gradual dense-to-sparse training paradigm used by (Liu et al., 2021a) is not directly comparable to RigL or other similar end-to-end sparse DST methods. Zhou et al. (2021) explored how N:M sparsity can be achieved during training using magnitude-based pruning during the forward pass and a Straight-Through Estimator (STE) (Bengio et al., 2013) on the backward pass. In their method, the dense network weights are projected into a sparse network during each training iteration. The sparse network is obtained by selecting the top-N out of every M contiguous weights and STE is used to propagate the approximated gradients through the projection function. However, in their initial experiments sparse networks trained with STE exhibited a significant performance drop compared to a dense benchmark. The authors conjectured that the reduced perfor-

mance could be due the gradients approximation performed by STE resulting in sparse connectivity instabilities during training. To counteract this, Zhou et al. (2021) introduced a regularization term applied to the gradients of pruned weights and called their approach Sparse-Refined Straight-Through Estimator (SR-STE). Their results include N:M ratios of 1:4, 2:4, 2:8, 4:8, 1:16, corresponding to model sparsities of 25%, 50%, 75% and 93.75%. Although SR-STE utilizes sparse operations in the forward pass and can find sparse models optimized for inference, it does not reduce the training cost significantly. Specifically, SR-STE training requires (1) storing original parameters in their dense format, and (2) calculating dense gradients during each training iteration. This makes SR-STE training as expensive as the original dense training in terms of memory and compute cost¹. On the other hand, DST methods such as RigL, and our proposed method SRigL, were developed for end-to-end sparse training and use sparse parameters and gradients throughout training.

Accelerating Fine-grained N:M Structured Sparsity Nvidia (2020) introduced the Ampere Tensor Core GPU architecture (e.g. A100 GPUs) and proposed the 2:4 fine-grained structured sparsity scheme that enables SNNs to be accelerated on this hardware *at inference time*. This scheme places a constraint on the allowed sparsity pattern: For every contiguous array of four weights, two are pruned, yielding a 50%-sparse net. The resulting regular structure of the weight matrix allows one to compress it efficiently and to reduce memory storage and bandwidth by operating on the nonzero weights only. Since the focus is on acceleration at inference time, the authors proposed to use the standard method of magnitude-based pruning post training to achieve the 2:4 sparsity. Importantly, this work considered exclusively the 2:4 ratio; other N:M ratios cannot be accelerated on Ampere GPUs.

3. Method

Most existing sparse-to-sparse DST methods, including the state-of-the-art — RigL — learn an *unstructured* sparse mask, and yet structured sparsity realizes substantially better acceleration in practice. Our goal in this work is to introduce structural constraints on the sparse mask learned by RigL, in order to make it more amenable to acceleration while not affecting RigL’s generalization performance. Constant fan-in represents a special case of N:M sparsity where N is the number of non-zero weights per neuron and M is the dense fan-in for each neuron within a given layer. We start with a theoretical analysis to explore the effect of various sparsity distributions with different degrees of structural constraints on the training dynamics of SNNs, motivating

¹To be precise, SR-STE can use some sparse operations and reduce training cost up to two thirds of the original dense training. However this is still far from fully sparse acceleration for training.

the particular structured sparsity we use.

3.1. Sparsity and Output-Norm Variance

Consider a SNN with ReLU activations, where each neuron has on average k connections to the previous layer (i.e., fan-in). It has been shown by Evci et al. (2022), that by normalizing the weights on initialization by a factor of $\sqrt{2/k}$, one achieves the following desirable normalization property for each layer ℓ with output z^ℓ :

$$\mathbb{E}\left(\frac{\|z^{\ell+1}\|^2}{\|z^\ell\|^2}\right) = 1,$$

meaning that on average the size of each layer output is constant. However, the variance of this ratio is non-trivial. In networks with large depth, it can accumulate, leading to exponentially large variance at the final layer (Li et al., 2021). Minimizing this variance on initialization has been shown to have a positive effect on training dynamics in some network models (Littwin et al., 2020), as it stabilizes the gradients. We therefore analyze the output norm variance as a guiding quantity for sparsity-type selection.

In the following, we consider three different types of sparsity distributions, which respectively correspond to different degrees of sparsity *structure* in the SNN, and derive analytic expressions for the behaviour of output norm variance in SNNs with the given sparsity type. The derivations for the following results can be found in Appendix A.

- **“Bernoulli sparsity”**: A connection between each neuron in layer $\ell+1$ and each neuron in layer ℓ appears *independently* with probability $p = \frac{k}{n}$, resulting in each neuron having k connections *on average* and each layer having nk connections *on average*. The variance is:

$$\text{Var}_{\text{Bernoulli}}\left(\frac{\|z^{\ell+1}\|^2}{\|z^\ell\|^2}\right) = \frac{5n-8+18\frac{k}{n}}{n(n+2)}. \quad (1)$$

- **“Constant Per-Layer sparsity”**: Exactly kn connections are distributed at random in the layer connecting the n neurons in layer $\ell+1$ and the n neurons in layer ℓ , resulting in each neuron having k connections *on average*. The variance is:

$$\text{Var}_{\text{Const-Per-Layer}}\left(\frac{\|z^{\ell+1}\|^2}{\|z^\ell\|^2}\right) = \frac{(n^2+7n-8)C_{n,k}+18\frac{k}{n}-n^2-2n}{n(n+2)}, \quad (2)$$

where $C_{n,k} = \frac{n-1/k}{n-1/n}$. Note that when $n \gg 1$, $C_{n,k} \approx 1 - \frac{n-k}{n^2k}$ is close to 1, and with $C_{n,k} = 1$ we recover the formula for Bernoulli sparsity, meaning that this sparsity type and Bernoulli sparsity are very similar.

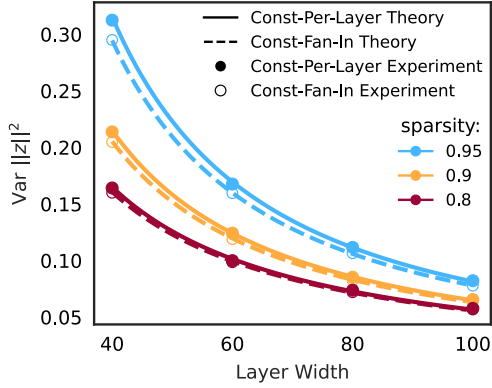


Figure 2: Output-norm Variance: Theoretical predictions and simulation results demonstrating that sparse layers with constant fan-in have consistently smaller output-norm variance than layers with the same number of non-zero weights but without the constant fan-in constraint. Note: Bernoulli type is not shown because the corresponding curve is almost identical to constant-per-layer type.

- **“Constant Fan-In sparsity”:** Each neuron in layer $\ell + 1$ is connected to exactly k neurons from layer ℓ , chosen uniformly at random. In this case, the variance is:

$$\text{Var}_{\text{Const-Fan-In}} \left(\frac{\|z^{\ell+1}\|^2}{\|z^\ell\|^2} \right) = \frac{5n - 8 + 18\frac{k}{n}}{n(n+2)} - \frac{3(n-k)}{kn(n+2)}. \quad (3)$$

In deriving the above results we assumed that the direction of the layer output vector $\frac{z^\ell}{\|z^\ell\|}$ is uniformly distributed on the unit sphere. We compare our theoretical predictions with simulations in Fig. 2 and verify their accuracy. Bernoulli and constant-per-layer distribution result in unstructured sparsity, and most of the current DST approaches, including RigL, operate with constant-per-layer sparsity. In contrast, the constant-fan-in type imposes a strong structural constraint. Therefore we are somewhat surprised to find that, in fact, constant-fan-in sparsity always produces slightly smaller output-norm variance than the other types. The difference is larger when $k \ll n$, i.e., for very sparse networks. This indicates that, at the very least, the constant fan-in constraint should not impair SNN training dynamics and performance, motivating our method of maintaining the constant fan-in sparsity constraint within a DST approach.

3.2. Structured RigL

As motivated by Section 3.1, we propose to enforce the constant-fan-in constraint within a sparse-to-sparse DST method to learn structured sparse connectivity from scratch. Specifically, we use RigL by Evci et al. (2021), which can obtain highly sparse networks with generalization performance comparable to their dense baselines.

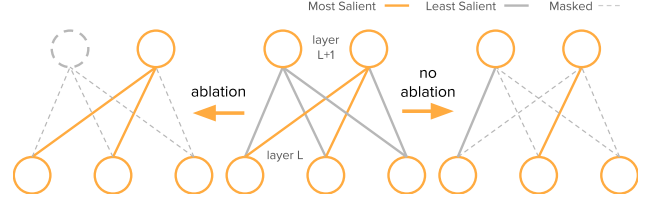


Figure 3: Neuron Ablation. At sparsity levels over 90%, RigL learns to completely mask (ablate) a large number of neurons within each layer, effectively reducing layer width. Imposing a constant fan-in constraint requires all neurons to have the same number of (non-pruned) incoming weights and therefore inhibits ablation, which results in worse generalization performance than RigL. Allowing SRigL to ablate neurons restores RigL-level performance.

In brief, the methodology of RigL is to update the SNN connectivity during training by *pruning* weights with the smallest magnitude and *regrowing* those with the largest corresponding gradient magnitude in *each* layer. This occurs in periodic, but relatively infrequent mask update steps throughout most of training. In SRigL, weight saliency must be determined at the *neuron level* (in convolutional layers, at the level of each filter), since we enforce that every neuron (output channel) has the same number of unmasked incoming weights (i.e. constant fan-in) (Fig. 1).

However, this approach alone lags behind RigL in generalization significantly at very high sparsities (>90%), as shown in Figs. 5a and 5b. This is because the constant fan-in constraint has an important side-effect: Under a strict constant fan-in constraint, neurons can never be entirely masked (ablated), as illustrated in Fig. 3. At very high sparsity levels this can lead to some neurons having only 1–2 weights, limiting their capacity to learn complex features and consequently reducing generalization performance. Indeed, at high sparsities we observed empirically that RigL reduces the width of the model at high sparsities to maintain generalization performance — we believe we are the first to explicitly identify this behaviour within a DST method.

To resolve this issue in SRigL, we implement a neuron ablation method, allowing SRigL to maintain both a constant fan-in constraint *and* to reduce layer width at high sparsities. The steps below outline our SRigL method.

In the following procedure, the first two steps are the same as in RigL, while the other steps are specific to SRigL, containing modifications to include the constant fan-in constraint and dynamic neuron ablation. We first set an ablation threshold defining the minimum percentage of salient weights per neuron. Then, for each layer we do the following:

1. Obtain magnitudes of the active weights and gradient magnitudes of the pruned weights; these will serve as prune and growth criteria, respectively.

2. Compute K , the number of weights to be grown and pruned in the current step in this layer. We always grow the same number of connections as we prune.
3. Count the number of salient weights per neuron. A weight is considered *salient* if it is in the top- K of either the largest-magnitude weights or the largest-magnitude gradients.
4. Ablate neurons that have less salient weights than the predefined minimum. Ablation is done by pruning all incoming weights. These pruned weights are redistributed to the remaining neurons in the following steps.
5. Compute the new fan-in constraint based on the number of ablated neurons.
6. Prune the K smallest-magnitude weights in the current layer.
7. For each active neuron, regrow as many weights as required, proceeding in order of decreasing gradient magnitude, until the target fan-in is achieved.

4. Results

We implement SRigL in PyTorch by extending an existing implementation of RigL (McCreary, 2020). We evaluate our method empirically on image classification tasks, training the ResNet-18 (He et al., 2016) and Wide ResNet-22 (Zagoruyko & Komodakis, 2017) models on the CIFAR-10 dataset (Krizhevsky, 2009), and the ResNet-50 model (He et al., 2016) on the 2012 ImageNet Large Scale Visual Recognition Challenge (ILSVRC-12) dataset (Russakovsky et al., 2015), commonly referred to as ImageNet. Unless noted otherwise, we use the same hyperparameter configuration as the original RigL method. The modified hyperparameters proposed by Liu et al. (2021b) may yield higher generalization performance, but a detailed investigation of the hyperparameters for SRigL is left to future work.

For all SRigL experimental results listed below we use 30% as the minimum percentage of salient weights per neuron unless otherwise noted. This value was selected based on a hyperparameter sweep performed by training ResNet-18 and Wide ResNet-22 on the CIFAR-10 dataset, see Appendix C.

4.1. ResNet-18 trained on CIFAR-10

Our training regimen follows Evci et al. (2021): We train each network for 250 epochs (97,656 steps) using a batch size of 128. An initial learning rate of 0.1 is reduced by a factor of 5 every 77 epochs (about 30,000 steps). We use stochastic gradient descent (SGD) with momentum, with an L2 weight decay coefficient of $5e-4$ and momentum coefficient of 0.9. For each trial, we select a desired sparsity in the range from 0.5 to 0.99. We achieve the desired overall sparsity by distributing the per-layer sparsity according to the Erdős-Rényi-Kernel (ERK) (Evci et al., 2021; Mocanu et al., 2018) distribution, which scales the per-layer sparsity based on the number of neurons and the dimensions of the convolutional kernel, if present. We set the number of training steps between connectivity updates ΔT to 100.

At each connectivity update, the portion of weights to be pruned or regrown is based on a cosine annealing schedule (Dettmers & Zettlemoyer, 2019) with an initial value $\alpha = 0.3$. The portion of weights to be updated decays from the initial value to zero once 75% of the total training steps have been completed, after which the weight mask remains constant. The minimum percentage of salient weights per neuron is set at 30% based on the results of a small grid search performed on CIFAR-10 with ResNet-18 and Wide ResNet-22. See Fig. 9 for details. We repeat training with five different random seeds for both methods and report the averages and standard deviation compared to a densely-connected benchmark model in Figure 5b and Table 1.

These results confirm that imposing a constant fan-in constraint during sparse training does not significantly

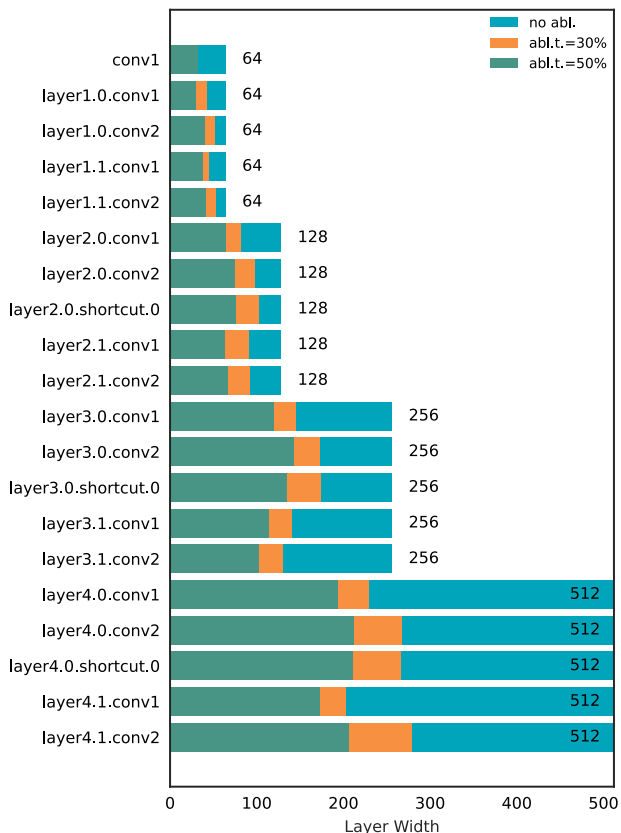


Figure 4: ResNet-18/CIFAR-10 layer widths at the end of training. Without ablation, constant fan-in constraint enforces that sparse layers retain their original width. When ablation is enabled, the user-defined ablation threshold (minimum percentage salient weights per neuron) is used to control the amount of ablation.

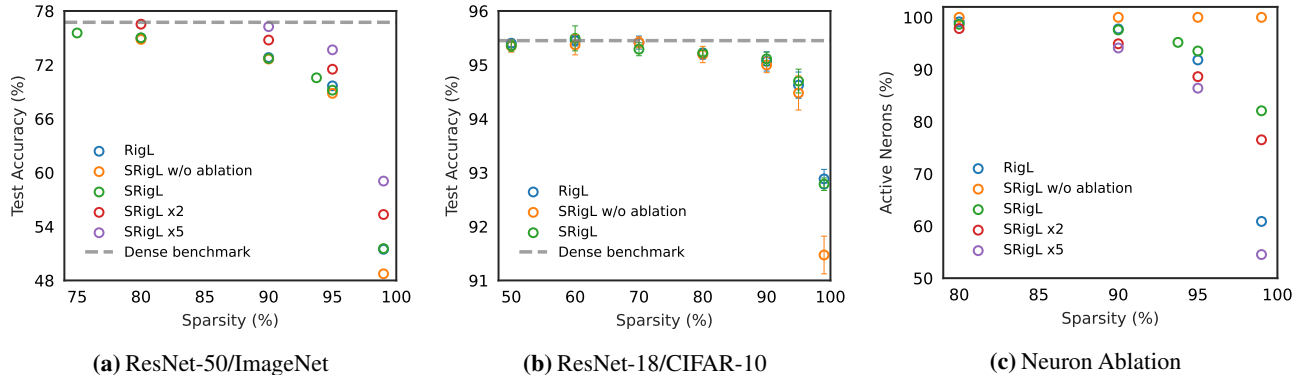


Figure 5: (a) ResNet-50/ImageNet Top-1 Test Accuracy when trained with SRigL for a range of sparsities is comparable to RigL. Extended training durations of x2 and x5 are also reported for SRigL. Results reported are single runs. (b) ResNet-18 Test Accuracy when trained with SRigL for a range of sparsities is comparable to RigL. The mean and 95% confidence intervals are shown for five different random seeds. (c) Neuron Ablation: The percentage active neurons (i.e., not ablated) following RigL/SRigL training. RigL ablates a large number of neurons at high sparsities.

Table 1: Test accuracy for ResNet-18 on CIFAR-10 trained with RigL or SRigL with/without neuron ablation at varying sparsities repeated with five different random seeds.

sparsity (%)	RigL	SRigL	
		w/o	w/ ablation
50	95.4±0.1	95.3±0.1	95.4±0.1
60	95.4±0.1	95.4±0.2	95.5±0.2
70	95.4±0.1	95.4±0.1	95.3±0.1
80	95.2±0.1	95.2±0.1	95.2±0.0
90	95.1±0.1	95.0±0.1	95.1±0.1
95	94.6±0.2	94.5±0.3	94.7±0.2
99	92.9±0.1	91.5±0.3	92.8±0.1
0	<i>dense ResNet-18:</i>		95.5

degrade generalization performance of the SNN compared to the RigL method. We inspect the connectivity of ResNet models trained with the RigL method and find, as shown in Fig. 5c, that at 95% sparsity 10.9% of neurons are removed completely. Thus, RigL results in fewer, but more densely connected neurons, whereas the fan-in constraint enforces that all neurons are retained.

In Fig. 4 we plot the number of neurons ablated at ablation thresholds of 0, 30, and 50% to demonstrate how the minimum percentage salient weights per neuron parameter can be used to guide the final model width during training.

4.2. ResNet-50 trained on ImageNet

Our training regimen for training on the ImageNet dataset follows Evci et al. (2021) with the exception of using a mini-batch size of 512 instead of 4096. We linearly scale the learning rate ΔT to account for our smaller batch size. Our learning rate uses a linear warm-up to reach a maximum

value of 0.2 at epoch five and is reduced by a factor of 10 at epochs 30, 70, and 90. Using a mini-batch of 512, we train the networks for 256,000 steps to match RigL’s training duration. Linearly scaling the learning rate in this manner was included in the original RigL source code and is further motivated by Goyal et al. (2018). We increase ΔT to 800 and average the dense gradients over eight mini-batch steps to ensure that SRigL has the same quality of parameter saliency information available as RigL. We use a cosine connectivity update schedule with $\alpha = 0.3$. We initialize the sparse model weights per Evci et al. (2022). We train the networks using SGD with momentum, L2 weight decay, and label smoothing (Szegedy et al., 2016) coefficients of 0.9, 1e-4 and 0.1, respectively. We set the minimum percentage of salient weights per neuron to 30% based on our grid search presented in Fig. 9.

We use the same standard data augmentation in our data preprocessing as RigL, including randomly resizing to 256×256 or 480×480 pixels, random crops to 224×224 pixels, random horizontal flips, and per-image normalization to zero mean and unit variance using identical per RGB channel mean and standard deviation values as RigL. We also investigate the effect of extended training with $\times 2$ and $\times 5$ the original number of training epochs.

Due to compute limitations, we train each model with a single seed and report the results in Fig. 5a and Table 2. SRigL yields similar generalization performance as RigL across each sparsity and training duration considered. At high sparsities, SRigL with ablation outperforms SRigL without ablation, highlighting the importance of dynamic neuron ablation as sparsity increases. RigL x5 results at 99% sparsity used a dense first layer, unlike all other results reported in Table 2. Despite this difference, SRigL x5 at 99% sparsity is comparable to the RigL x5 results. We expect that the 99% sparse models would be improved by using a

Table 2: Top-1 ImageNet test accuracy of ResNet-50 trained with RigL or SRigL at high sparsities and with various training times (as in Evci et al. (2021)), e.g. 5× more training epochs than dense ResNet-50.

sparsity (%)	RigL		SRigL			
	1×	5× [†]	w/o	w/ ablation		
			1×	1×	2×	5×
80	74.9	77.1	74.8	75.0	76.5	–
90	72.8	76.6	72.6	72.7	74.7	76.2
95	69.6	74.6	68.8	69.1	71.5	73.6
99	51.4	61.9 [‡]	48.7	51.5	55.3	59.0
0	<i>dense ResNet-50:</i>		76.7			

[†] 5× RigL results are from Evci et al. (2021)

[‡] uses a dense first layer at 99% sparsity, unlike other results

dense first layer for all SRigL results. Similar to RigL, we observe that SRigL generalization performance improves with increasing training time.

4.3. Wide ResNet-22/CIFAR-10

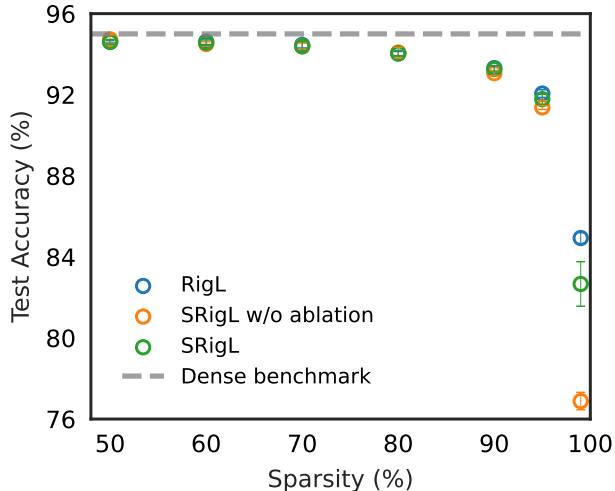
In Fig. 6 we present results of training WideResNet-22 (Zagoruyko & Komodakis, 2017) with RigL or SRigL on the CIFAR-10 dataset. The training details for this experiment are identical to those reported in Section 4.1. SRigL without ablation performs poorly at very high sparsities. With ablation, SRigL achieves generalization performance comparable to RigL.

4.4. FLOPs Analysis

In Fig. 7, we present an analysis of the FLOPs required during training and inference for SRigL and compare with SR-STE. We calculate FLOPs using the same methodology as Evci et al. (2021) by considering only operations induced by convolutional and linear layers and their activations. FLOPs for add and pooling operations are ignored. For training FLOPs, we also disregard FLOPs required for mask updates, as this step is amortized over ΔT steps and is negligible compared to the FLOPs required otherwise for training. The open-source code for counting operations is from the NeurIPS 2019 MicroNet Challenge and is available on GitHub².

Similar to other DST methods, SRigL obtains generalization performance comparable to a dense network benchmark at a fraction of the FLOPs required for both training and inference.

²https://github.com/google-research/google-research/tree/master/micronet_challenge



sparsity (%)	RigL	SRigL	
		w/o	w/ ablation
50	94.6±0.1	94.7±0.1	94.6±0.1
60	94.6±0.1	94.5±0.1	94.6±0.1
70	94.5±0.1	94.4±0.1	94.4±0.1
80	94.0±0.1	94.1±0.2	94.0±0.1
90	93.3±0.1	93.1±0.1	93.3±0.1
95	92.1±0.1	91.4±0.1	91.8±0.2
99	84.9±0.2	76.9±0.3	82.7±0.8
0	<i>dense Wide ResNet-22:</i>		95.0

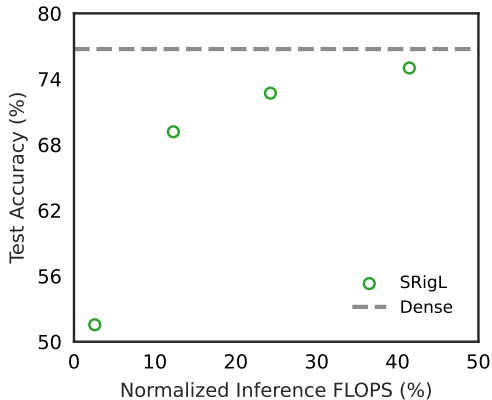
Figure 6 & Table 3: Test accuracy of Wide ResNet-22 trained on CIFAR-10. Mean and 95% confidence intervals are reported over five runs.

Table 4: SRigL Sparsity and FLOPs for training and inference.

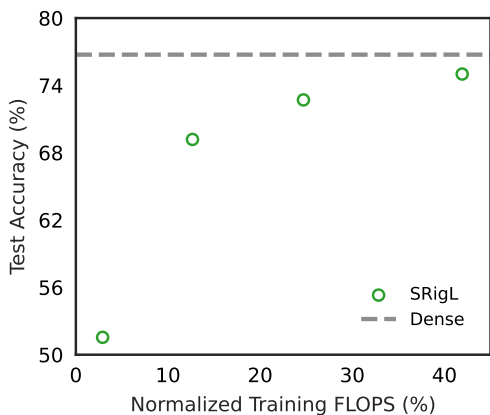
sparsity (%)	SRigL FLOPs	
	Training (×1e18)	Inference (×1e9)
80	1.13	3.40
90	0.77	1.99
95	0.40	1.01
99	0.09	0.21
0	3.15	8.20

4.5. Acceleration of Constant Fan-in Sparsity

Although commodity hardware can accelerate some types of N:M sparsity (Nvidia, 2020), the specific type of sparsity we propose to learn with SRigL — constant fan-in sparsity — has seen less attention. Theoretical speedups (i.e. FLOPs) are limited in demonstrating the real-world acceleration potential of a proposed sparse representation in general, and yet conversely creating a fully-optimized software or hardware implementation of a novel representation typically requires significant engineering effort outside of the scope of this paper.



(a) Inference FLOPs



(b) Training FLOPs

Figure 7: (a) Inference FLOPs for SRigL and SR-STE on ResNet-50/ImageNet at a variety of sparsities. FLOPs are normalized by dense inference FLOPs.

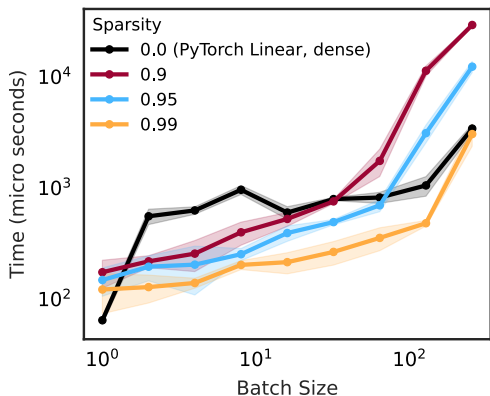


Figure 8: PyTorch Timings Benchmarking a naive (non-optimized) PyTorch implementation of our condensed representation on CPU (Intel(R) Xeon(R) CPU E5-2690 v3 @ 2.60GHz, 48 threads on 24 cores).

Here we show that even a straight-forward PyTorch implementation of our proposed condensed neural network representation (see Appendix B) can demonstrate this real-world acceleration on CPU. In Fig. 8, we present real-world timings comparing the `torch.nn.Linear` layer and our condensed linear layer, which works as a drop-in replacement. We report mean timings and standard deviations across a minimum of five forward passes for a single condensed layer at sparsities of 99%, 95%, and 90% and a standard dense PyTorch Linear layer. For both the condensed and dense layer, we use a single layer with 10 neurons. We vary the batch size between 1 to 256 and use 65,536 features in our input tensor. The input tensors consist of 32 bit floating point values and the convolutional weight tensors are in a channel-first layout typical to PyTorch (batch size, channels, height, width). At high sparsity levels and moderate batch sizes, the condensed layer outperforms the dense `torch.nn.Linear` layer moderately. This result is highly promising, since it is reasonable to expect that a more optimized software implementation and/or explicit hardware support would improve upon these results significantly.

5. Conclusion

In this work we present SRigL, a novel dynamic sparse training that learns a variant of structured N:M sparsity. SRigL is capable of end-to-end sparse training while maintaining generalization performance on par with state-of-the-art unstructured sparse training methods. By enforcing a constant fan-in constraint on the learned topology of our networks, the models are amenable to hardware acceleration similar to 2:4 sparsity currently available on NVIDIA GPUs. Our observation that RigL ablates neurons at high sparsities inspires our dynamic neuron ablation method which enables SRigL to match the performance of RigL at high sparsities. We present preliminary timings using an non-optimized implementation of our condensed representation which compare well against a dense layer. We hope this work will motivate future work implementing additional fine-grained structured sparsity schemes within the DST framework.

6. Acknowledgements

We acknowledge the support of the Natural Sciences and Engineering Research Council of Canada (NSERC) and Alberta Innovates. We also acknowledge the helpful feedback of Trevor Gale.

References

Bengio, Y., Léonard, N., and Courville, A. Estimating or propagating gradients through stochastic neurons for conditional computation. 2013.

- Dettmers, T. and Zettlemoyer, L. Sparse Networks from Scratch: Faster Training without Losing Performance. Technical Report arXiv:1907.04840, arXiv, August 2019.
- Devlin, J., Chang, M.-W., Lee, K., and Toutanova, K. BERT: Pre-training of Deep Bidirectional Transformers for Language Understanding, May 2019. URL <http://arxiv.org/abs/1810.04805>. arXiv:1810.04805 [cs].
- Dietrich, A. S. D., Gressmann, F., Orr, D., Chelombiev, I., Justus, D., and Luschi, C. Towards Structured Dynamic Sparse Pre-Training of BERT. January 2022. URL <https://openreview.net/forum?id=-e7awdzWsOc>.
- Elsen, E., Dukhan, M., Gale, T., and Simonyan, K. Fast sparse convnets. In *Proceedings of the IEEE/CVF Conference on Computer Vision and Pattern Recognition (CVPR)*, 2020.
- Evcı, U., Gale, T., Menick, J., Castro, P. S., and Elsen, E. Rigging the Lottery: Making All Tickets Winners. Technical Report arXiv:1911.11134, arXiv, July 2021. arXiv:1911.11134.
- Evcı, U., Ioannou, Y., Keskin, c., and Dauphin, Y. Gradient Flow in Sparse Neural Networks and How Lottery Tickets Win - AAAI 2022 Poster, February 2022.
- Gale, T., Zaharia, M., Young, C., and Elsen, E. Sparse gpu kernels for deep learning, 2020.
- Goyal, P., Dollár, P., Girshick, R., Noordhuis, P., Wesolowski, L., Kyrola, A., Tulloch, A., Jia, Y., and He, K. Accurate, large minibatch sgd: Training imagenet in 1 hour, April 2018.
- Han, S., Pool, J., Tran, J., and Dally, W. Learning both weights and connections for efficient neural network. In *Advances in neural information processing systems*, 2015.
- Han, S., Mao, H., and Dally, W. J. Deep compression: Compressing deep neural network with pruning, trained quantization and huffman coding. In *4th International Conference on Learning Representations, ICLR 2016, San Juan, Puerto Rico, May 2-4, 2016, Conference Track Proceedings*, 2016.
- He, K., Zhang, X., Ren, S., and Sun, J. Deep Residual Learning for Image Recognition. In *2016 IEEE Conference on Computer Vision and Pattern Recognition (CVPR)*, pp. 770–778, Las Vegas, NV, USA, June 2016. IEEE. ISBN 978-1-4673-8851-1. doi: 10.1109/CVPR.2016.90.
- Hoefler, T., Alistarh, D., Ben-Nun, T., Dryden, N., and Peste, A. Sparsity in Deep Learning: Pruning and growth for efficient inference and training in neural networks. *arXiv:2102.00554 [cs]*, January 2021. URL <http://arxiv.org/abs/2102.00554>. arXiv: 2102.00554.
- Jiang, P., Hu, L., and Song, S. Exposing and Exploiting Fine-Grained Block Structures for Fast and Accurate Sparse Training. In *Proceedings of the Neural Information Processing Systems Conference (NeurIPS)*, October 2022. URL <https://openreview.net/forum?id=sFapsu4hYo>.
- Krizhevsky, A. Learning multiple layers of features from tiny images. Technical report, 2009.
- Li, M., Nica, M., and Roy, D. M. The future is log-gaussian: Resnets and their infinite-depth-and-width limit at initialization. In Beygelzimer, A., Dauphin, Y., Liang, P., and Vaughan, J. W. (eds.), *Advances in Neural Information Processing Systems*, 2021.
- Littwin, E., Myara, B., Sabah, S., Susskind, J., Zhai, S., and Golan, O. Collegial ensembles. In Larochelle, H., Ranzato, M., Hadsell, R., Balcan, M., and Lin, H. (eds.), *Advances in Neural Information Processing Systems*, volume 33, pp. 18738–18748. Curran Associates, Inc., 2020.
- Liu, S., Chen, T., Chen, X., Atashgahi, Z., Yin, L., Kou, H., Shen, L., Pechenizkiy, M., Wang, Z., and Mocanu, D. C. Sparse Training via Boosting Pruning Plasticity with Neuroregeneration. In *Advances in Neural Information Processing Systems*, volume 34, pp. 9908–9922. Curran Associates, Inc., 2021a.
- Liu, S., Yin, L., Mocanu, D. C., and Pechenizkiy, M. Do We Actually Need Dense Over-Parameterization? In-Time Over-Parameterization in Sparse Training. In *Proceedings of the 38th International Conference on Machine Learning*, pp. 6989–7000. PMLR, July 2021b. URL <https://proceedings.mlr.press/v139/liu21y.html>. ISSN: 2640-3498.
- McCreary, D. Pytorch implementation of rigging the lottery: Making all tickets winners, Nov 2020. Re-implementation/extension of the work done by Google Research: <https://github.com/google-research/rigl>.
- Mocanu, D. C., Mocanu, E., Stone, P., Nguyen, P. H., Gibescu, M., and Liotta, A. Scalable training of artificial neural networks with adaptive sparse connectivity inspired by network science. *Nature Communications*, 9(1):2383, December 2018. ISSN 2041-1723. doi: 10.1038/s41467-018-04316-3.
- Nikdan, M., Pegolotti, T., Iofinova, E., Kurtic, E., and Alistarh, D. SparseProp: Efficient Sparse Backpropagation for Faster Training of Neural Networks, February 2023. URL <http://arxiv.org/abs/2302.04852>. arXiv:2302.04852 [cs].
- Nvidia. Nvidia A100 Tensor Core GPU Architecture. Technical report, Nvidia, 2020.

- Russakovsky, O., Deng, J., Su, H., Krause, J., Satheesh, S., Ma, S., Huang, Z., Karpathy, A., Khosla, A., Bernstein, M., Berg, A. C., and Fei-Fei, L. Imagenet large scale visual recognition challenge. *International Journal of Computer Vision (IJCV)*, 2015.
- Szegedy, C., Vanhoucke, V., Ioffe, S., Shlens, J., and Wojna, Z. Rethinking the Inception Architecture for Computer Vision. pp. 2818–2826, June 2016. doi: 10.1109/CVPR.2016.308. ISSN: 1063-6919.
- Wang, C., Zhang, G., and Grosse, R. Picking winning tickets before training by preserving gradient flow. In *ICLR, 2020*.
- Yang, L., Meng, J., Seo, J.-s., and Fan, D. Get More at Once: Alternating Sparse Training with Gradient Correction. In *Proceedings of the Neural Information Processing Systems Conference (NeurIPS)*, October 2022. URL <https://openreview.net/forum?id=lYZQRpQLesi>.
- Zagoruyko, S. and Komodakis, N. Wide Residual Networks, 2017. arXiv:1605.07146.
- Zhou, A., Ma, Y., Zhu, J., Liu, J., Zhang, Z., Yuan, K., Sun, W., and Li, H. Learning n:m fine-grained structured sparse neural networks from scratch. In *International Conference on Learning Representations, 2021*.

A. Computing the Output Norm Variance

Definition A.1. Let $\xi \in \{0,1\}^N$ be a binary vector. Let $I \in \{0,1\}^{N \times N}$ be an $N \times N$ binary matrix. Let $u \in \mathbb{R}^N$ be any vector. Let $W \in \mathbb{R}^{N \times N}$ be a matrix of iid $\mathcal{N}(0,1)$ random variables.

Define the vector z by:

$$z = \sqrt{\frac{2}{k}} (W \odot I) (\xi \odot u) \quad (4)$$

i.e. the entries z_i are given by:

$$z_i = \sqrt{\frac{2}{k}} \sum_{j=1}^n W_{ij} I_{ij} \xi_j u_j \quad (5)$$

Proposition A.2. The variance of each entry z_i is:

$$\text{Var}(z_i) = \frac{2}{k} \sum_{j=1}^n I_{ij} \xi_j u_j^2 \quad (6)$$

and therefore the distribution of each z_i can be written as

$$z_i \stackrel{d}{=} g_i \sqrt{\frac{2}{k} \sum_{j=1}^n I_{ij} \xi_j u_j^2} \quad (7)$$

where g_i are N iid $\mathcal{N}(0,1)$ random variables.

Proof. By the properties of variance:

$$\text{Var}(z_i) = \frac{2}{k} \sum_{j,j'} I_{ij} I_{ij'} \xi_j \xi_{j'} u_j u_{j'} \text{Cov}(W_{ij}, W_{ij'}) \quad (8)$$

$$= \frac{2}{k} \sum_{j,j'} I_{ij} I_{ij'} \xi_j \xi_{j'} u_j u_{j'} \delta_{j=j'} \quad (9)$$

$$= \frac{2}{k} \sum_j I_{ij}^2 \xi_j^2 u_j^2 \quad (10)$$

$$= \frac{2}{k} \sum_j I_{ij} \xi_j u_j^2 \quad (11)$$

since $I_{ij}^2 = I_{ij}$ and $\xi_j^2 = \xi_j$ because they are binary valued. Once the variance is established, notice that z_i is a linear combination of Gaussians with $z_i \perp z_{i'}$, because the row $W_{ij} \perp W_{i'j}$. Hence the z_i are independent Gaussians, so the form $z_i \stackrel{d}{=} g_i \sqrt{\frac{2}{k} \sum_{j=1}^n I_{ij} \xi_j u_j^2}$ follows. \square

Corollary A.3. The norm $\|z\|^2$ can be written as:

$$\|z\|^2 \stackrel{d}{=} \frac{2}{k} \sum_{i,j=1}^n g_i^2 I_{ij} \xi_j u_j^2 \quad (12)$$

Proposition A.4 (“Bernoulli Sparsity”). Suppose that $u \in \mathbb{R}^n$ is uniform from the unit sphere, the entries $I_{ij} \sim \text{Ber}(\frac{k}{n})$, $\xi_j \sim \text{Ber}(\frac{1}{2})$ all independent of each other. Then:

$$\mathbb{E}(\|z\|^2) = 1 \quad (13)$$

$$\text{Var}(\|z\|^2) = \frac{5n-8+18\frac{n}{k}}{n(n+2)} \quad (14)$$

Proof. We have

$$\mathbb{E}(\|z\|^2) = \frac{2}{k} \sum_{i,j=1}^n \mathbb{E}[g_i^2 I_{ij} \xi_j u_j^2] \quad (15)$$

$$= \frac{2}{k} \sum_{i,j=1}^n \mathbb{E}[g_i^2] \mathbb{E}[I_{ij}] \mathbb{E}[\xi_j] \mathbb{E}[u_j^2] \quad (16)$$

$$= \frac{2}{k} \sum_{i,j=1}^n 1 \cdot \frac{k}{n} \cdot \frac{1}{2} \cdot \frac{1}{n} \quad (17)$$

$$= 1 \quad (18)$$

Similarly, we compute the 4-th moment as follows:

$$\mathbb{E}(\|z\|^4) = \left(\frac{2}{k}\right)^2 \sum_{i,j,i',j'}^n \mathbb{E}[g_i^2 g_{i'}^2] \mathbb{E}[I_{i'j'} I_{ij}] \mathbb{E}[\xi_j \xi_{j'}] \mathbb{E}[u_j^2 u_{j'}^2] \quad (19)$$

We split this into four cases and evaluate these based on whether or not $i = i'$ and $j = j'$ in the following table.

Case	Num. Terms	$\mathbb{E}[g_i^2 g_{i'}^2]$	$\mathbb{E}[I_{i'j'} I_{ij}]$	$\mathbb{E}[\xi_j \xi_{j'}]$	$\mathbb{E}[u_j^2 u_{j'}^2]$
$i = i', j = j'$	n^2	3	$\frac{k}{n}$	$\frac{1}{2}$	$\frac{3}{n(n+2)}$
$i \neq i', j = j'$	$n^2(n-1)$	1	$\left(\frac{k}{n}\right)^2$	$\frac{1}{2}$	$\frac{3}{n(n+2)}$
$i = i', j \neq j'$	$n^2(n-1)$	3	$\left(\frac{k}{n}\right)^2$	$\left(\frac{1}{2}\right)^2$	$\frac{1}{n(n+2)}$
$i \neq i', j \neq j'$	$n^2(n-1)^2$	1	$\left(\frac{k}{n}\right)^2$	$\left(\frac{1}{2}\right)^2$	$\frac{1}{n(n+2)}$

Table 5: Overview of terms for Bernoulli type sparsity.

Combining the value of each term with the number of terms gives the desired result for the variance. \square

Proposition A.5 (“Constant-per-layer sparsity”). *Suppose that $u \in \mathbb{R}^n$ is uniform from the unit sphere and $\xi_j \sim \text{Ber}(\frac{1}{2})$ are independent of each other. Suppose the entries of the matrix I_{ij} are chosen such that:*

There are exactly kn ones and exactly $n^2 - nk$ zeros in the matrix I , and their positions in the matrix are chosen uniformly from the $\binom{n^2}{nk}$ possible configurations. Then:

$$\mathbb{E}(\|z\|^2) = 1 \quad (20)$$

$$\text{Var}(\|z\|^2) = \frac{(n^2 + 7n - 8)C_{n,k} + 18\frac{k}{n} - n^2 - 2n}{n(n+2)} \quad (21)$$

Proof. Note that $\mathbb{E}(I_{ij}) = k/n$ still holds, since there are kn ones distributed over n^2 locations. Thus the computation for $\mathbb{E}(\|z\|^2)$ is identical to the previous proposition. Note also that when there are two entries, we have:

$$\mathbb{E}[I_{ij} I_{i'j'}] = \begin{cases} \frac{k}{n} & \text{if } i = i' \text{ and } j = j' \\ \frac{k}{n} \cdot \frac{nk-1}{n^2-1} & \text{otherwise} \end{cases} \quad (22)$$

$$= \begin{cases} \frac{k}{n} & \text{if } i = i' \text{ and } j = j' \\ \left(\frac{k}{n}\right)^2 \cdot C_{n,k} & \text{otherwise} \end{cases} \quad (23)$$

where $C_{n,k} = \frac{n-1/k}{n-1/n}$. The table with terms for computing $\mathbb{E}(\|z\|^4)$ becomes: The extra factor of $C_{n,k}$ in the entries leads

to the stated result. \square

Case	Num. Terms	$\mathbb{E}[g_i^2 g_{i'}^2]$	$\mathbb{E}[I_{i'j'} I_{ij}]$	$\mathbb{E}[\xi_j \xi_{j'}]$	$\mathbb{E}[u_j^2 u_{j'}^2]$
$i = i', j = j'$	n^2	3	$\frac{k}{n}$	$\frac{1}{2}$	$\frac{3}{n(n+2)}$
$i \neq i', j = j'$	$n^2(n-1)$	1	$\left(\frac{k}{n}\right)^2 C_{n,k}$	$\frac{1}{2}$	$\frac{3}{n(n+2)}$
$i = i', j \neq j'$	$n^2(n-1)$	3	$\left(\frac{k}{n}\right)^2 C_{n,k}$	$\left(\frac{1}{2}\right)^2$	$\frac{1}{n(n+2)}$
$i \neq i', j \neq j'$	$n^2(n-1)^2$	1	$\left(\frac{k}{n}\right)^2 C_{n,k}$	$\left(\frac{1}{2}\right)^2$	$\frac{1}{n(n+2)}$

Table 6: Overview of terms for Constant-per-layer type sparsity.

Proposition A.6 (“Constant Fan-In sparsity”). *Suppose that $u \in \mathbb{R}^n$ is uniform from the unit sphere, and $\xi_j \sim \text{Ber}(\frac{1}{2})$ all independent of each other. Suppose the entries of the matrix I_{ij} are chosen so that:*

1. *There are exactly k ones in each row of the matrix I and exactly $n-k$ zeros in the matrix I , chosen uniformly from the $\binom{n}{k}$ possible ways this can happen.*
2. *Different rows of I are independent.*

Then:

$$\mathbb{E}(\|z\|^2) = 1 \quad (24)$$

$$\text{Var}(\|z\|^2) = \frac{5n-8+18\frac{n}{k}}{n(n+2)} - \frac{3(n-k)}{kn(n+2)} \quad (25)$$

Proof. Same arguments as before apply, but now we have

$$\mathbb{E}[I_{ij} I_{i'j'}] = \begin{cases} \frac{k}{n} & \text{if } i = i' \text{ and } j = j' \\ \frac{k}{n} \frac{k-1}{n-1} & \text{if } i = i' \text{ and } j \neq j' \\ \left(\frac{k}{n}\right)^2 & \text{otherwise} \end{cases} \quad (26)$$

$$(27)$$

and the table for the variance computation becomes:

Case	Num. Terms	$\mathbb{E}[g_i^2 g_{i'}^2]$	$\mathbb{E}[I_{i'j'} I_{ij}]$	$\mathbb{E}[\xi_j \xi_{j'}]$	$\mathbb{E}[u_j^2 u_{j'}^2]$
$i = i', j = j'$	n^2	3	$\frac{k}{n}$	$\frac{1}{2}$	$\frac{3}{n(n+2)}$
$i \neq i', j = j'$	$n^2(n-1)$	1	$\left(\frac{k}{n}\right)^2$	$\frac{1}{2}$	$\frac{3}{n(n+2)}$
$i = i', j \neq j'$	$n^2(n-1)$	3	$\frac{k}{n} \cdot \frac{k-1}{n-1}$	$\left(\frac{1}{2}\right)^2$	$\frac{1}{n(n+2)}$
$i \neq i', j \neq j'$	$n^2(n-1)^2$	1	$\left(\frac{k}{n}\right)^2$	$\left(\frac{1}{2}\right)^2$	$\frac{1}{n(n+2)}$

Table 7: Overview of terms for Constant-fan-in type sparsity.

Which leads to the stated result. □

$$(28)$$

B. Condensed Matrix Multiplication

Using a constant fan-in sparse representation presents an advantage compared to the general N:M sparse representation in that we can represent our weight matrices in a compact form, since every neuron/convolutional filter has the same number of non-zero weights. Here we demonstrate how this can be used to accelerate a fully-connected layer.

Consider the standard matrix-vector product:

$$Wv = \begin{pmatrix} W_{11} & W_{12} & \dots & W_{1d} \\ W_{21} & W_{22} & \dots & W_{2d} \\ \vdots & \vdots & \ddots & \vdots \\ W_{n1} & W_{n2} & \dots & W_{nd} \end{pmatrix} \begin{pmatrix} v_1 \\ v_2 \\ \vdots \\ v_d \end{pmatrix} = \begin{pmatrix} \sum_{j=1}^L W_{1j} v_j \\ \sum_{j=1}^L W_{2j} v_j \\ \vdots \\ \sum_{j=1}^L W_{nj} v_j \end{pmatrix} = v^{\text{out}} \quad (29)$$

When W is sparse and has only k non-zero elements per row, the sums representing each element of v^{out} will be limited to k terms, i.e.:

$$v_i^{\text{out}} = \sum_{\alpha=1}^k W_{i j_\alpha} v_{j_\alpha} \quad \text{with } j_\alpha \in \{1, \dots, n_{\text{in}}\}, j_\alpha \neq j_{\alpha'} \quad (30)$$

Note that the expression on the right-hand side of Eq. (29) can be represented as an operation between a dense matrix $W^c \in \mathbb{R}^{n_{\text{out}} \times k}$ (we call it ‘‘condensed W ’’) and k vectors $v^{\pi_1}, \dots, v^{\pi_k}, v^{\pi_i} \in \mathbb{R}^{n_{\text{out}}}$, whose elements are drawn from v with replacement (we call them ‘‘recombinations of v ’’). The operation is a sum over element-wise products between the i -th column of W^c and the i -th column vector v^{π_i} :

$$Wv = \sum_{i=1}^k W_{:,i}^c \odot v^{\pi_i} \quad (31)$$

Mathematically, these methods are equivalent for any matrices. Computationally, the condensed method can be more efficient, in particular for sparse matrices with constant small fan-in k . By construction, this method requires the sparse matrix W to be stored in dense representation which involves two 2D arrays of shape $n_{\text{out}} \times k$: One holds the *values* of the non-zero elements of W and the other one their respective *column indices*, which are used to generate input vector re-combinations. An efficient computational implementation of this method is subject of ongoing work on this project. Based on our results, the constant fan-in constraint does not appear to have a limiting effect on SNNs.

C. Minimum Salient Weights per Neuron

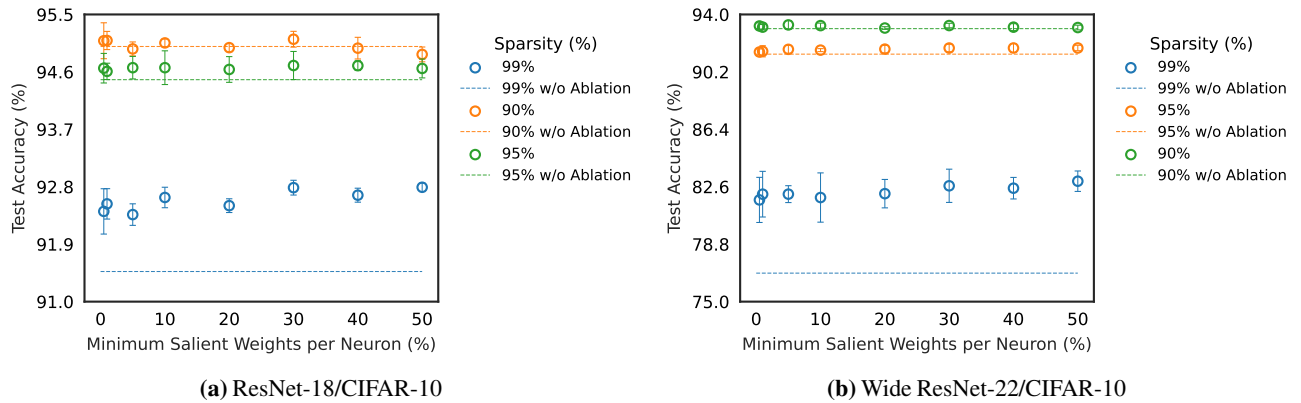


Figure 9: (a) ResNet18/CIFAR-10 Test Accuracy vs. Minimum Salient Weights per Neuron when trained with SRigL with and without ablation for a range of sparsities. The mean and 95% confidence intervals are shown for five different random seeds for the runs with ablation. For the runs without ablation, we report the mean of five different random seeds. **(b) Wide ResNet-22 Test Accuracy vs. Minimum Salient Weights per Neuron.** The mean and 95% confidence intervals are shown for five different random seeds.

Fig. 9 depicts the generalization performance of highly sparse ResNet-18 and Wide ResNet-22 models trained on the CIFAR-10 dataset. SRigL’s generalization performance at high sparsities is improved with dynamic neuron ablation; however, the specific value selected for minimum salient weights per neuron does not have a significant effect on performance. Our experiments demonstrate that SRigL performs well with a variety of minimum salient weights per neuron values. In Section 4

we report the results of SRigL models trained with minimum salient weights per neuron set to 30%. With dynamic ablation enabled, we set the minimum salient weight per neuron to 1 if the user-defined threshold results in a value less than one. In Fig. 10, many layers in ResNet-50 are set to the minimum threshold of one when we apply a minimum salient percentage of 30%. This minimum threshold explains the invariance of the model’s performance when comparing against multiple values for minimum salient percentage weights per neuron.

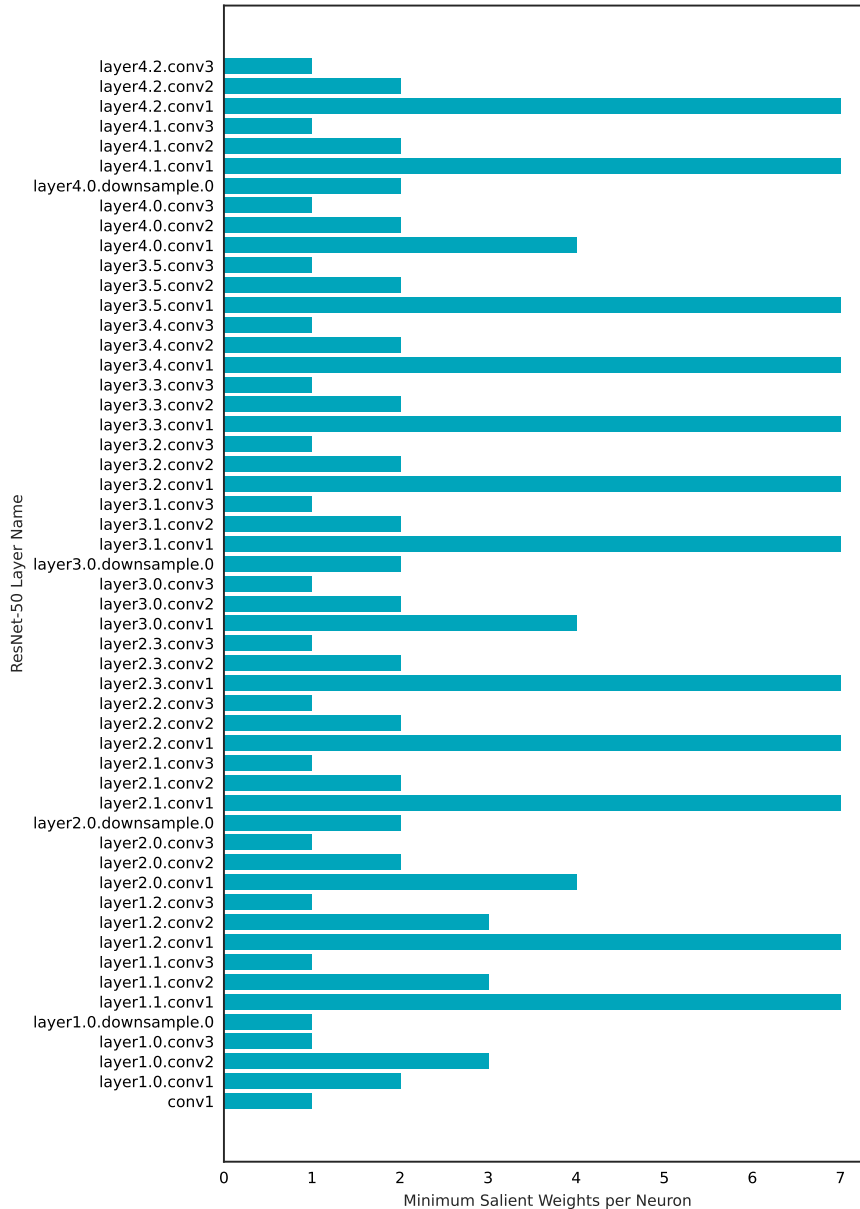


Figure 10: ResNet-50 Layer vs. Minimum salient weights per neuron. SRigL sets the minimum salient weight per neuron to 1 if the product between the user-defined minimum percentage salient weights per neuron and the sparse fan-in per neuron is less than 1. Therefore, even in a relatively large network such as ResNet50 many of the layers only require that a single weight be active to keep the neuron active. We believe this is why SRigL’s performance is relatively invariant to various ablation thresholds.

D. SparseProp Backend Benchmarks

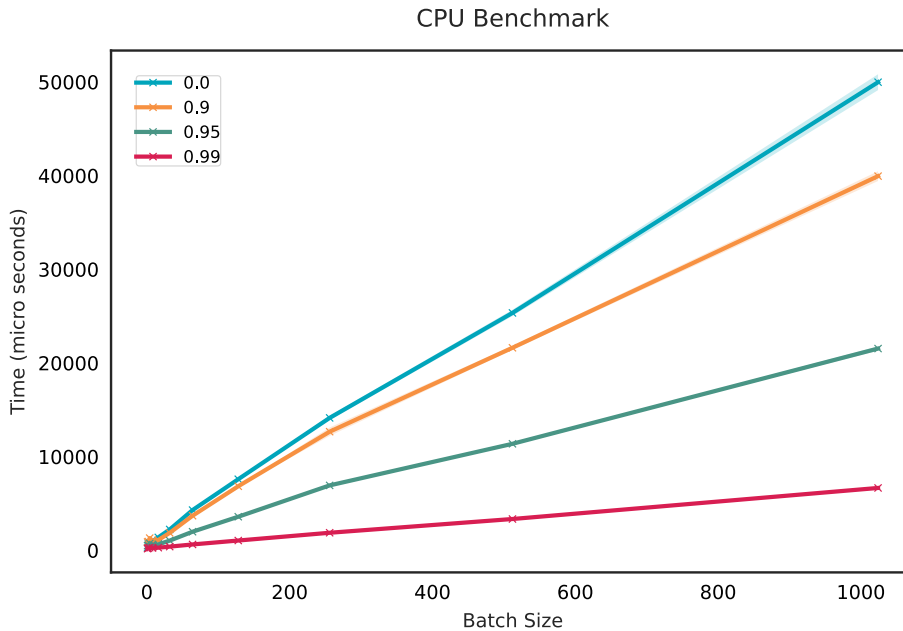


Figure 11: SparseProp Timings Benchmarking our condensed representation on CPU with the SparseProp backend (Intel(R) Xeon(R) E5-2683 v4 @ 2.10GHz).

Our straight-forward PyTorch implementation is only faster than the linear layer benchmark at sparsities of 99% as demonstrated in Fig. 8. However, since our condensed representation GEMM algorithm was implemented in python directly, it suffers significant overhead compared to C++ or CUDA backends. Here we demonstrate that the SparseProp (Nikdan et al., 2023) C++ backend is capable of accelerating our sparse models in real-world settings. We report mean timings and standard deviations across a minimum of five forward passes for a single condensed layer with SparseProp backend at sparsities of 99%, 95%, and 90% and a standard dense PyTorch Linear layer. Both the condensed and linear layer are based on the linear classifier in a ResNet-50 model. The layers have 1000 neurons and we use an input tensor with 2048 features. We vary the batch size between 1 to 1024. The input tensors consist of 32 bit floating point values and the convolutional weight tensors are in a channel-first layout typical to PyTorch (batch size, channels, height, width). This result is highly promising since the SparseProp backend does not utilize the constant fan-in constraint. Additional acceleration is expected with a suitable backend designed to exploit the constant fan-in constraint.